MATERIALS SCIENCE

A new approach to both high safety and high performance of lithium-ion batteries

Shanhai Ge, Yongjun Leng, Teng Liu, Ryan S. Longchamps, Xiao-Guang Yang, Yue Gao, Daiwei Wang, Donghai Wang, Chao-Yang Wang*

We present a novel concept to achieve high performance and high safety simultaneously by passivating a Li-ion cell and then self-heating before use. By adding a small amount of triallyl phosphate in conventional electrolytes, we show that resistances of the passivated cells can increase by ~5×, thereby ensuring high safety and thermal stability. High power before battery operation is delivered by self-heating to an elevated temperature such as 60°C within tens of seconds. The present approach of building a resistive cell with highly stable materials and then delivering high power on demand through rapid thermal stimulation leads to a revolutionary route to high safety when batteries are not in use and high battery performance upon operation.

INTRODUCTION

Rechargeable lithium-ion batteries (LIBs) are widely used in electrified vehicles, consumer electronics, and stationary energy storage systems. Simultaneous realization of high safety and high energy density/performance is a perpetual pursuit. Unfortunately, conventional batteries are passive devices where the performance, safety, and calendar/cycle life are all dictated by the electrochemical reactivity at ever-present anode/electrolyte and cathode/electrolyte interfaces. An inherent conflict between the reactivity and stability of battery materials persists at the electrode/electrolyte interfaces (EEIs). More specifically, highly reactive electrode/electrolyte materials provide high power and high performance but result in poor safety and accelerated degradation even when the battery is not in use. Highly stable (i.e., less reactive) electrode/electrolyte materials give rise to battery safety, low degradation, low self-discharge, and long life, but such materials offer low power and performance. As a result, materials development for batteries has always aimed at trade-offs of finding electrode and electrolyte materials that are not too reactive but also not too stable.

This work describes a new strategy to achieve both safe and energy-dense battery (SEB) cells, as schematically sketched in Fig. 1, where the cell resistance is plotted against the inverse of temperature. First, a passivated cell is judiciously designed and built by using highly stable materials and by creating exceptionally stable EEIs, as characterized by higher charge-transfer resistance (R_{ct}) and higher direct-current resistance (DCR). This is illustrated in Fig. 1 by the line from point a (the conventional Li-ion cell design) to point b (the SEB cell design). It follows that these resistive SEB cells are inherently stable and safe, as demonstrated by nail penetration, short circuiting, and high-temperature storage. Second, in order for SEB cells to deliver high power during operation, they are heated instantaneously before operation, say from room temperature to 60°C, so as to recover acceptable operational DCR and ultimately battery power, going from point b (at room temperature) to point c (at an elevated temperature such as 60°C) in Fig. 1. This power on demand through rapid thermal stimulation is opposed to standby power in the present-day LIB cells, where the high-power EEIs need to be ever present. Rapid cell heating at a speed of 1° to 5°C/s has been made possible by a self-heating structure discovered by Wang *et al.* (*1*), in which a micrometer-thick nickel foil is inserted in a stack of anode-separator-cathode assemblies for uniform and internal heating. Thus, heating from room temperature to 60°C for battery operation conveniently takes only 10 to 20 s.

To achieve the requisite stable, robust EEIs, the additive, triallyl phosphate (TAP), is used in this work based on sufficient evidence in the literature of its ability to improve cell stability at both high-voltage and high-temperature conditions. For example, in 2015, Xia *et al.* (*2*) demonstrated that a TAP-based electrolyte forms thick protective layers on both electrodes in graphite/NCM442-based cells as evidenced by reduced self-discharge at high temperatures, reduced gas production during high-temperature cycling, and increased R_{ct}. Although TAP has been explored previously, it is chosen in the present work to create resistive Li-ion cells as an example to illustrate the concept of realizing high safety and high performance simultaneously. Other ways to build resistive cells, such as using electrode materials of low Brunauer-Emmett-Teller areas, are effective as well.

RESULTS

As a proof of concept, we prepare a baseline cell composed of a standard electrolyte, 1 M $LiPF_6$ in ethylene carbonate (EC)/ethyl methyl carbonate (EMC) (3/7 wt) + 2 weight % (wt %) vinylene carbonate (VC), and a graphite anode and an NCM622 cathode. Protective layers of solid electrolyte interphase (SEI) on graphite and cathode electrolyte interphase (CEI) are formed during initial charge/discharge cycles. To yield low DCR and hence high power, these interfacial layers are usually thin, lacking sufficient density and resilience to resist decomposition under abuse conditions, to suppress continuous reaction of the solvent EC in the SEI, or to hinder continuous oxidation of EC with oxygen released from cathode materials in the CEI, thereby leading to Li consumption and loss of cell capacity. In contrast, in SEB cells, we create highly stable, flame-retardant EEIs through the addition of a small amount of TAP in the standard electrolyte. This electrolyte modification is accompanied by the simultaneous reduction of EC content, i.e., EC/EMC (1/9 wt) + 2 wt % VC, intended for further reduction in gas production via side reactions. In this work, we present results for three prototype SEB cells, identified as SEB-1,

Electrochemical Engine Center and Department of Mechanical Engineering, Pennsylvania State University, University Park, PA 16802, USA.
*Corresponding author. Email: cxw31@psu.edu

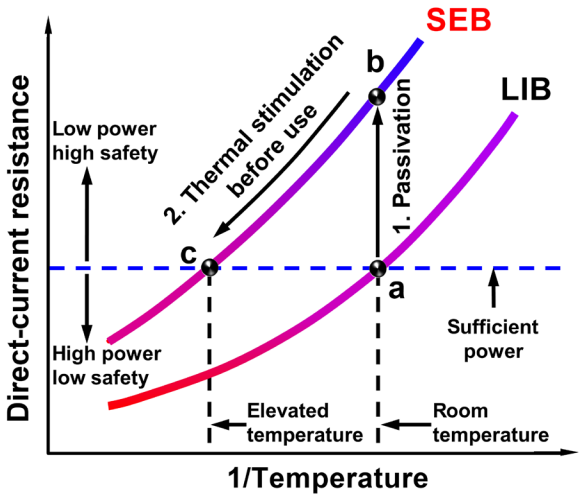

Fig. 1. Principles and advantages of a SEB versus a conventional LIB. DCR is shown to vary with the inverse of temperature for both batteries, where the upper curve for the passivated SEB is always safer due to higher DCR. The SEB can, however, achieve a similar power output to the LIB by thermal stimulation before operation, shown as going from point b to c.

SEB-2, and SEB-3 and corresponding to 0.5, 1, and 1.5 wt % TAP, respectively. The charge-transfer resistance of the SEB cells, measured by electrochemical impedance spectroscopy (EIS), increases by 3× to 5× as compared to the baseline cell without the electrolyte additives, as shown in Fig. 2A. The high impedance comes from the polymerization of TAP molecules that form thick and dense interfacial films at the surfaces of both the anode and cathode (*2*). On the anode side, the film serves as an enhanced SEI layer to stabilize further growth. On the cathode side, the film hinders EC in the electrolyte from reacting with lattice oxygen on the NCM surface at high temperature or high voltage (*3*), as shown schematically in Fig. 2B.

PolyTAP and its composites are flame-retardant materials. In addition, the PolyTAP has electrically insulative properties and stability at elevated temperatures (*4*). All these properties make PolyTAP well suited to enhance the safety of SEB cells under abuse conditions. This is confirmed by nail penetration tests shown in Fig. 2C, where the temperature rise is only 100°C (without cell deformation, smoking, or fire) versus almost 1000°C (catching fire) in the baseline case (Fig. 2D). The superior safety performance of the SEB cell is further illustrated by the electrical performance of the cell during nail penetration. For the baseline cell, the cell voltage decreases to 0.1 V within 5 s after the nail penetration. The sharp voltage drop indicates that the shorting current is extremely high due to low internal resistance of the baseline cell. In contrast, the voltage of the SEB cell drops from 4.171 to 3.085 V within 5 s after penetration, showing a slow and controlled discharge due to the high internal resistance of the SEB cell. The substantially higher resistance in the SEB cell than the baseline is caused by the electrically nonconductive layers formed on the surface of the graphite and NCM particles, as schematically shown in Fig. 2B.

The stability and safety of SEB cells are further evident in high-voltage charge and high-temperature calendar life tests (figs. S1 and S2). The SEB cells can undergo 1254 exposures to high-voltage abuse [constant current (CC) charge to 4.4 V, constant voltage (CV) to C/20] at 40°C with a capacity retention of 80%, whereas the baseline cell sustains only 40 cycles at the same capacity loss and operating temperature, indicating that the SEB cell is >30× more stable and hence safer than the baseline cells under high-voltage charging conditions. Calendar life testing further shows that the passivated SEB cells can effectively suppress self-discharge. The self-discharge current is measured by holding the cell voltage constant at a required value, such as 4.187 V for 100% state of charge (SOC). Both baseline and SEB cells display a fast decrease of self-discharge current density in the beginning of calendar aging due to anode SEI layer growth. Fresh SEB cells show self-discharging currents ~5× lower than the baseline cell at room temperature and 50% SOC, 6× lower at room temperature and 100% SOC, and ~7× lower at 60°C at both 50 and 100% SOC. After 60 days of storage, the self-discharge current begins to plateau; however, the self-discharge current in the SEB cell is still 2× lower than that in the baseline cell at room temperature and 50% SOC and 3× lower at room temperature and 100% SOC. The self-discharge becomes 4× lower at high temperature (60°C) at both 50 and 100% SOC, indicating that at elevated temperatures, the SEB cells maintain superiority in calendar life over the baseline cell.

A distinctive feature of SEB cells is high power on demand. When batteries are not in operation, SEB cells are left idle at room temperature, exhibiting high stability and safety. However, upon operation, a SEB cell switches to high-reactivity conditions through rapid thermal stimulation. This can be illustrated through DCR, which is inversely proportional to power performance. Here, DCRs upon discharge and charge for SEB and baseline LIB cells are measured at 50% SOC by a 10-s hybrid pulse power characterization (HPPC) method. As expected, the DCR values increase substantially by adding a small amount of TAP in the electrolyte, as shown in Fig. 3 (A and B), which also demonstrates that adding more TAP in SEB-3 (e.g., 1.5 wt %) results in a further increase in DCR, owing to the formation of thicker protective layers.

Figure 3C shows the relative power of SEB cells versus the baseline LIB, where the power of the baseline cell at room temperature is normalized to be unity, thus demonstrating that SEB cells can provide sufficient, higher power by operating at higher temperatures. At 50% SOC, SEB-1 operated at 29.2°C provides the same power as the baseline cell at room temperature. The safest cell, SEB-3, with 1.5 wt % TAP additive requires an operation temperature of 44.6°C to deliver the same power as the baseline cell at room temperature. The baseline cell has a narrow temperature window of 15° to 35°C, whereas the SEB cells have much higher maximum operating temperature without becoming excessively reactive. Thus, the necessity of higher temperature operation for power recovery does not pose an issue for SEB cells. At 50% SOC, the discharge power boost over the baseline Li-ion cell is 2.05, 1.81, and 1.39 for the SEB-1, SEB-2, and SEB-3, respectively (Fig. 3C). Moreover, at the ambient temperature of 0°C, the baseline LIB cell has a relative power of 0.38, while SEB-2 has a relative power of 1.81 when operated at 60°C [it takes 30 s to heat up a cell from 0° to 60°C at a speed of 2°C/s, typical of the self-heating structure of Wang *et al.* (*1*)]. This is ~5× boost in power over the LIB cell for SEB cells working in the freezing environments. Generally, SEB cells perform independent of ambient temperatures or weather, as they are always heated up in a matter of seconds and operate at a constant elevated temperature. Although heating a cell to an elevated temperature consumes cell energy, the total deliverable energy of a cell, counterintuitively, is not reduced. As shown in fig. S3, the C/3 discharge energy was 9.62 watt-hours (Wh) for the baseline cell at room temperature and 10.15 Wh for the SEB-3 cell at 60°C. According to our previous

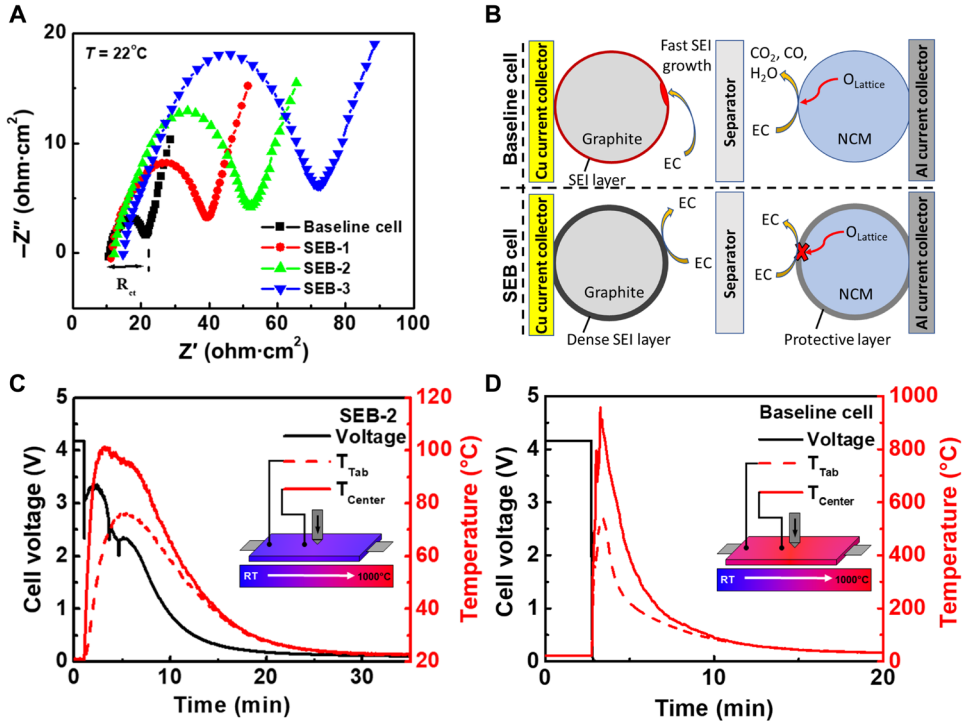

Fig. 2. Experimental comparison between LIB and SEB and mechanism explanation. (**A**) Nyquist plots showing measured charge-transfer resistances of SEB cells versus the baseline LIB cell. (**B**) Schematic showing the in situ formed interfacial layers on the surface of graphite and NCM particles. The enhanced SEI layer on graphite slows down EC transport though the film and suppresses further SEI growth. The CEI layer hinders EC oxidation with lattice oxygen over the NCM surface at high temperatures or high voltages. (**C** and **D**) Cell voltage and temperature evolutions during nail penetration of a SEB cell and the baseline LIB cell along with qualitative temperature distributions. Both cells are 2.8-Ah pouch cells composed of the same graphite anode and NMC622 cathode materials. The baseline LIB cell is filled with a standard electrolyte: 1 M $LiPF_6$ in EC/EMC (3/7 wt) + 2 wt % VC. The SEB cell has the electrolyte of 1 M $LiPF_6$ in EC/EMC (1/9 wt) + 2 wt % VC with TAP as electrolyte additive. RT, room temperature.

work (*1*), it takes ~1% cell energy for a 10°C temperature rise, meaning that the SEB-3 cell needs 3.5% of its energy for heating from 25° to 60°C; the remaining discharge energy is thus 9.79 Wh, which is 2% higher than that of the baseline cell at room temperature.

As mentioned, such rapid heating is achieved through the insertion of a micrometer-thick nickel sheet. The impact of this additional component on cell power density can be evaluated through Eq. 1, where *m* is the mass of the given cell and the ratio of discharge power evaluated through HPPC is inversely proportional to the ratio of DCRs

$$\frac{(\text{Power Density})_{\text{SEB}}}{(\text{Power Density})_{\text{baseline@RT}}} = \left(\frac{\text{DCR}_{\text{baseline@RT}}}{\text{DCR}_{\text{SEB@60°C}}}\right)\left(\frac{m_{\text{baseline}}}{m_{\text{SEB}}}\right) \quad (1)$$

The addition of the nickel foil increases cell mass by 1.3%, while the ratio of DCRs in Eq. 1 is the relative power presented in Fig. 3C at 60°C. On the basis of these values, the power density is not reduced but rather increased by a factor of 2.02, 1.79, and 1.37 in the case of SEB-1, SEB-2, and SEB-3, respectively. Thus, in the case of SEB-3 with the highest internal resistance, the power density is still 37% higher than the baseline cell operated at room temperature.

Figure 3D presents the relative interfacial reactivity as derived from the charge-transfer resistance of EIS results. This further confirms that increased operational temperature effectively decreases the charge-transfer resistance of SEB cells and consequently increases the cell reactivity and power. The reactivity boost over the baseline LIB cell is 2.06 for SEB-2. Overall, both relative power and relative reactivity illustrate the ability of SEB cells to achieve high power on demand. On the other hand, the values of relative reactivity of these two cells shown in Fig. 3D indicate that the SEB cell will be 5× safer and undergo 5× less aging at room temperature, which is supported by self-discharge and capacity retention tests displayed in fig. S2. Furthermore, the comparison of relative reactivity for the two cell types at 60°C indicates that the SEB cell is more than 2× less prone to thermal runaway.

Beyond safety and high power, there is an ever-increasing need for long cycle life of LIBs. Low-reactivity SEB cells built with highly stable materials offer longer calendar life (fig. S2), evident from the slow capacity fade when the battery is in idle conditions at room temperature. At elevated temperatures, cycling of SEB cells is also stable. Figure 4A compares capacity retention of the baseline cell with SEB cells during cycling at 60°C of 1C CC charge to 4.2 V CV charge till C/20 and then 1C discharge to 2.8 V. Clearly, the SEB cells outperform the baseline cell as evidenced by a 20% capacity loss at 481 cycles with visible signs of cell deformation due to gas evolution and graphite anode swelling for the baseline cell, while SEB-3 can achieve 2821 cycles before reaching 20% capacity loss. This corresponds to ca. 6× improvement in cycle life. In addition, SEB-3 achieves 4014 cycles at 75% capacity retention while still showing signs of a healthy cell capable of cycling stably (no perceptible gassing or lithium plating). The average discharge capacity of these 4014 cycles is 84.2% of an equivalent full cycle (EFC). Assuming a 153-mile

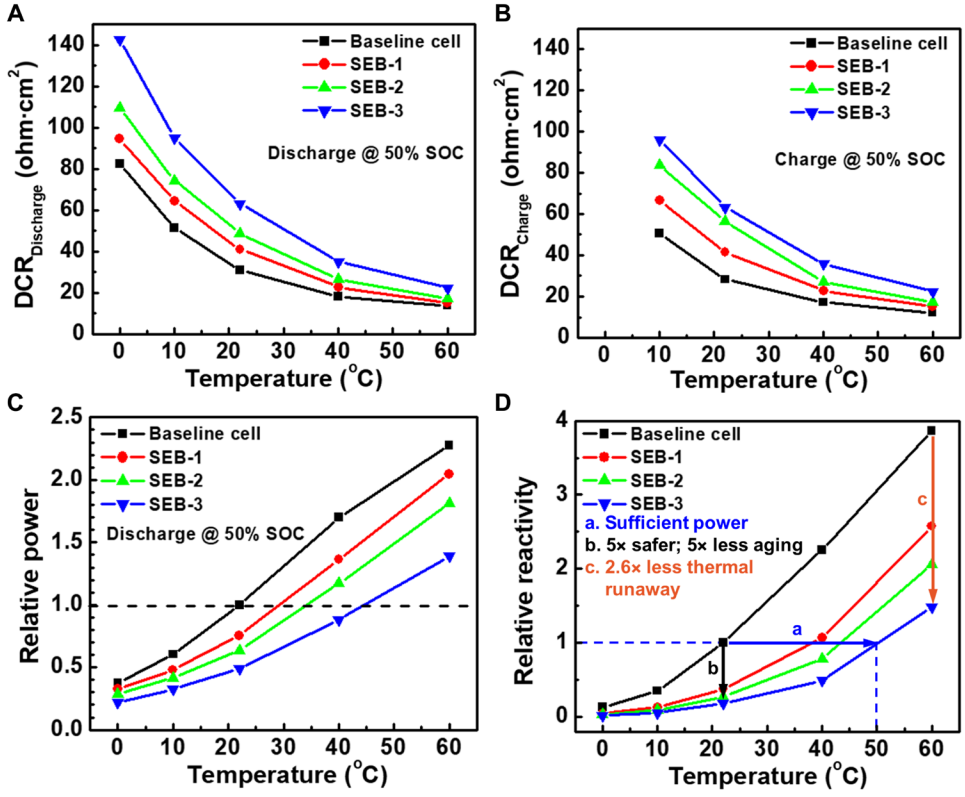

Fig. 3. Temperature dependence of cell power performance. (**A** and **B**) DCRs of discharge and charge, respectively, at 50% SOC for SEB cells versus the baseline LIB cell. (**C**) Relative discharge power ($DCR_{baseline@RT}/DCR$) of a SEB cell versus the baseline LIB cell. (**D**) Relative reactivity ($R_{ct,baseline@RT}/R_{ct}$) of a SEB cell versus the baseline LIB cell, showing that SEB cells operated at appropriate elevated temperatures, e.g., SEB-3 at 50°C, can deliver sufficient power at all ambient temperatures (labeled as line a), that SEB cells are 5× safer and less aging at room temperature (labeled as line b), and that SEB cells are 2.6× less prone to thermal runaway at 60°C (labeled as line c).

driving range per EFC for an electric vehicle (e.g., 2019 BMW i3), the 4014 cycles mean >517,000 miles of lifetime. That is more than 5× the warranty for commercial electric cars (e.g., BMW i3, 70% capacity for 8 years or 100,000 miles). Improvement of cell lifetime can be further demonstrated by considering the rate of capacity fade during calendar aging at room temperature (i.e., the stable state), which is 7× lower than that at 60°C (the reactive state). The SEB cell will only be heated to the reactive state for situations requiring high power or fast charging. The greater part of its lifetime (>90%) would be spent in idle conditions (the stable state). Therefore, in the field, the SEB cycle life is expected to extend much beyond 4014 cycles before reaching 25% capacity loss.

The tremendous extension of cycle life of the SEB over the baseline cell may stem from the denser and more stabilized SEI layer formed on graphite particles and CEI layer on NCM622 particles in the presence of the electrolyte additives. For the baseline cell, the nickel-rich NCM particles are prone to microcracks along grain boundaries (*5*, *6*) that provide gaps for electrolyte penetration and lead to more severe electrolyte oxidation and rock salt formation (*7*). Particle cracking also sets free new, fresh surface area from which oxygen can be released (*8*). The microcracks on NCM622 particles for the baseline cell are observed after only 50 cycles (Fig. 5D). The formation of cracks becomes much more notable throughout the micrograph domain after 956 cycles (Fig. 5F). For the SEB cells, cracks on NCM particles are not observed at 50 cycles, and a small amount of cracks are observed after 4021 cycles (Fig. 5J). The presence of microcracks not only causes a loss of contact but also accelerates NCM capacity fade. For the SEB cells, the polymer coating from TAP likely forms a robust CEI, reducing formation of microcracks (Fig. 2B). This is also evidenced by optical images (fig. S4) and no observable cell deformation or swelling after 4021 cycles even at an elevated temperature of 60°C.

The use of the TAP additives altered the EEI compositions markedly. We performed x-ray photoelectron spectroscopy (XPS) on the graphite and NCM electrodes after 4021 cycles and compared the EEI structure of the samples from the baseline cell after 956 cycles. At the graphite anode, the TAP-containing electrolyte-derived SEI contains high concentrations of C, O, and P elements, compared to the control sample of the baseline cell (Fig. 6 and fig. S5). In addition, a higher content of C─C species in the entire C-containing species was also found in the TAP-containing electrolyte-derived SEI, suggesting the decomposition of the TAP at the anode (fig. S5). Meanwhile, the composition of the cathode CEI was also changed. With the TAP additive, the SEI layer has more C, P, and F and less Li and O, compared to the baseline SEI (Fig. 6 and fig. S5). High contents of LiF and P-containing species (O─P═O, $Li_xP_yOF_z$, and $Li_xP_yF_z$) (*9*) were found in the cathode CEI layer, owing to the use of the TAP additive (Fig. 6). A detailed peak interpretation is as follows: peaks at 284.6, 286.1, 288.8, and 290.1 eV in the C 1s spectrum are attributed to C─C, C─O, O─C═O, and poly(O─C═O) (*10*), respectively; peaks at 684.6 eV in the F 1s spectrum are attributed to LiF; peaks at 686.9 eV in the F 1s spectrum and 136.7 eV in the

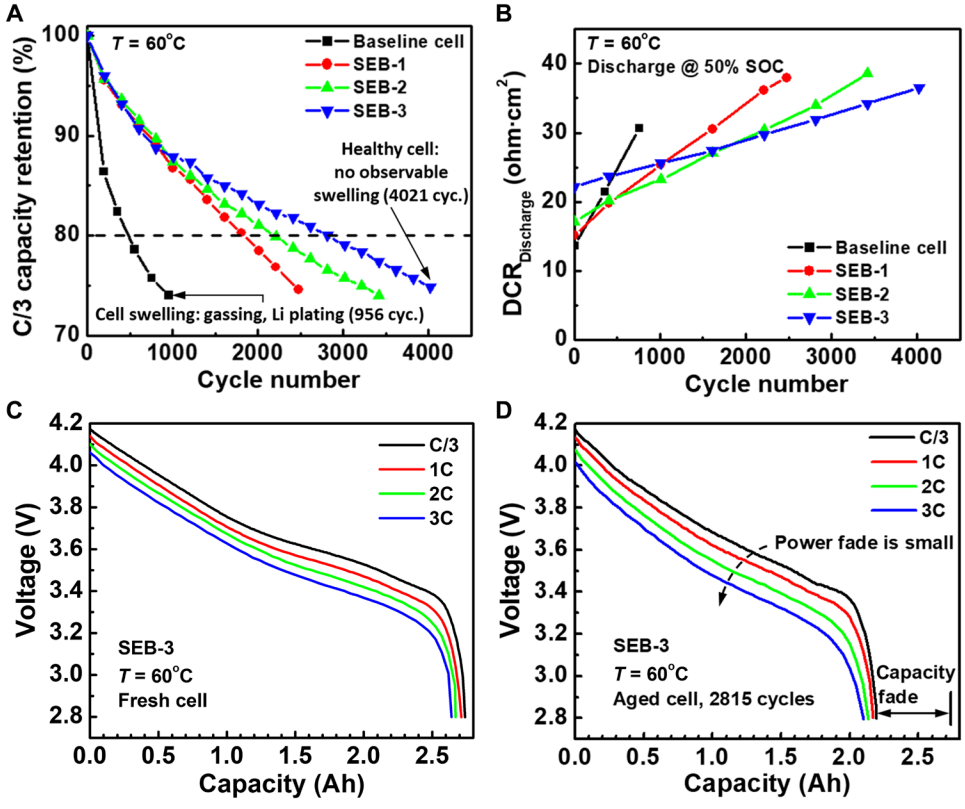

Fig. 4. Comparison of cycling stability at 60°C. (**A** and **B**) Capacity retention and DCR of the SEB cells versus the baseline LIB cell during cycling at 60°C. The cells are charged with CCCV protocol at 1 C to 4.2 V with a cutoff current of C/20 and then discharged at 1 C to 2.8 V. (**C** and **D**) Discharge curves of the fresh SEB cell versus aged cell.

P 2p spectrum are attributed to O—P═O and $Li_xP_yOF_z$; and peaks at 686.3 eV in the F 1s spectrum and 134.5 eV in the P 2p spectrum are attributed to $Li_xP_yF_z$. In comparing O 1s spectrum of the aged baseline (956 cycles) and SEB-3 electrodes (4021 cycles), the peak at 529.2 eV for SEB-3 cathode is effectively eliminated in comparison to that for the baseline cathode (Fig. 6). This indicates that less lattice oxygen of NCM622 is detected for SEB-3 cathode attendant to a relatively thicker CEI layer. This is consistent with the thicker CEI layer detected by Xia *et al.* (*2*) on the coated NMC442 surface in the presence of TAP additive. Thus, the XPS result confirms that the TAP additive leads to a thick CEI layer and, in consequence, slower crack evolution, less gas generation, and longer cycle life.

The three SEB cells show very close rates of capacity fade within 1000 cycles (Fig. 4A). Beyond 1000 cycles, SEB-3 shows a much lower rate of capacity fade than the other two SEB cells, as expected from its lowest reactivity. In comparison with the baseline cell, the stability and long cycle life of SEB cells are clearly evident, the reasons of which can be delineated from the differences in the capacity retention trend at various stages of aging. For the baseline cell, we see a sharp decrease in C/3 capacity retention during the initial stage and a slow decrease in the secondary stage. This is primarily attributed to the loss of lithium inventory during the quick and slow growth of the SEI layer. For the SEB cells, the capacity fade is linear with cycle number, indicating that there is no quick growth in the initial stage of aging as SEI layer growth is suppressed by in situ formation of the flame-retardant protective layer. Moreover, a sharp, nonlinear capacity loss due to lithium plating can usually be observed in the baseline cell at room temperature and at low temperatures in final stages of cell aging (*11*). In all SEB cells operated at 60°C, this lithium plating-induced capacity loss is, however, absent, indicative of no lithium plating in SEB cells. The SEB cell free of Li plating offers a significant improvement in safety over conventional LIB cells.

There is another advantage of SEB cells promising for ultralong cycle life when deployed in the field. While conventional LIB cells undergo a large environmental temperature swing, the SEB cells almost always operate at a single, constant temperature (say 60°C) regardless of ambient temperatures and after an extremely short period of initial transition by self-heating (on the order of tens of seconds). The latter feature guarantees minimal damage of battery materials in SEB cells caused by wide temperature variations.

For the baseline cell, the capacity loss at elevated temperatures is mainly due to SEI growth on the anode side and solvent oxidation on the cathode side. As a consequence, the DCR increases markedly with cycle number (Fig. 4B). In the case of SEB cells, the DCR of the fresh cell is initially much larger than the baseline cell; however, its rate of increase is much slower due to the protective coating on both the anode and cathode (Fig. 2B). Figure 4 (C and D) shows discharge curves of the fresh SEB cell versus the aged cell, respectively. Because of its DCR increase with cycle number, SEB-3 shows slight power fade after 2821 cycles at 60°C. In contrast, the baseline cell shows a drastic DCR increase and, hence, substantial power loss within only 556 cycles (fig. S6). For all the SEB cells with TAP additive, their DCRs increase linearly and increased additive content leads to higher DCR in fresh cells but slower DCR evolution with cycle number (Fig. 4B). The SEB cells do not produce gas during cycling tests, yielding more safety than the baseline cell. In addition,

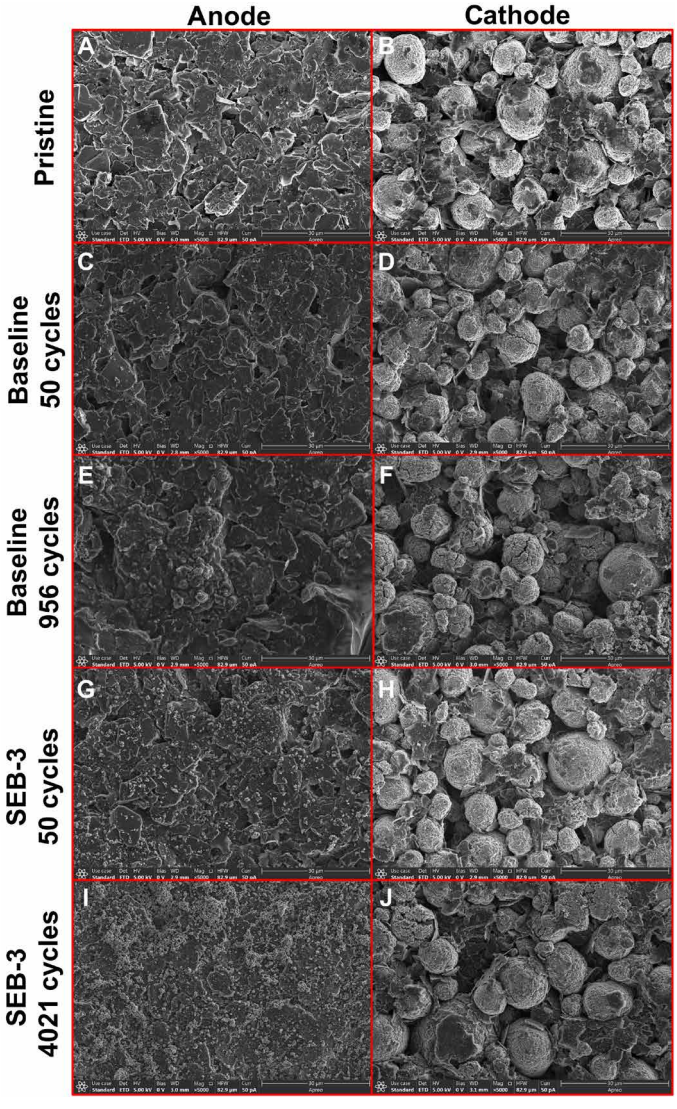

Fig. 5. SEM micrographs of the pristine, aged electrodes for the baseline and SEB-3 cells. (**A**) Pristine anode. (**B**) Pristine cathode. (**C**) Baseline anode after 50 cycles. (**D**) Baseline cathode after 50 cycles. (**E**) Baseline anode after 956 cycles. (**F**) Baseline cathode after 956 cycles. (**G**) SEB-3 anode after 50 cycles. (**H**) SEB-3 cathode after 50 cycles. (**I**) SEB-3 anode after 4021 cycles. (**J**) SEB-3 cathode after 4021 cycles. ETD, Everhart-Thornley Detector; HV, electron accelerating voltage; WD, working distance; HFW, horizontal field width.

cells containing TAP produce less gas during formation than the baseline cell (*2*, *12*).

Because of the high-voltage tolerance of SEB cells, when charged to a high voltage of 4.4 V as compared to 4.2 V, the SEB cell discharge capacity increases 12.7%, and its discharge energy increases 14.5% (fig. S1B). Thus, the high-voltage tolerance can be used to increase cell energy density.

The electrolytes for SEB cells were formulated by reducing EC content and adding TAP as an additive. Although EC is an essential solvent for SEI layer formation, it also leads to gas generation, especially at high voltage (*13*). Calendar aging testing shows that high-temperature and high-SOC conditions accelerate capacity fade and increase in internal resistance while also promoting gas generation. SEB cells initially contains 10 wt % EC in the electrolyte. Some EC is consumed during the formation cycle, resulting in an EC content much less than 10% in formed SEB cells. This is advantageous since the rate of gas generation in an EC-less electrolyte would be lower than that in an electrolyte with high EC content.

With the introduction of new materials into the electrolyte, the effect on cell cost, weight, and fabrication should be evaluated. The electrolyte additive, TAP, has a comparable price and density when compared to current standard solvents; thus, no notable material cost difference is expected with the introduction of SEB electrolytes. Unlike superconcentrated electrolytes (*14*), the electrolytes with TAP do not increase the viscosity compared to the standard electrolyte. From a fabrication perspective, the SEB electrolytes will also add no additional cost due to the similarity in processing during and after introduction into a cell.

Last, the SEB cells offer an important benefit associated with thermal management of a battery pack. When high power is required, the SEB cells are to be heated internally (*1*) and operated at elevated temperatures. Assuming the environmental temperature is 25°C, and the SEB and baseline cells operate at 60° and 30°C, respectively, the SEB provides a temperature difference driving heat dissipation that is 7× larger than the baseline case. Further, the SEB cell has lower DCR at its operational temperature of 60°C (17.1 ohm·cm^2 for SEB with 1 wt % TAP) than the baseline cell at 30°C (25.3 ohm·cm^2), indicating ~1.5× lower heat generation at the same current. The combination of these two factors eases the burden of thermal management by a factor of approximately 10 for SEB cells.

DISCUSSION

Overall, the novel SEB offers high safety and stability at idle conditions, demonstrated through mechanical (nail penetration), electrical (high-voltage charge), and thermal abuse (high-temperature storage). The stability of the SEB-2 cell under high voltage leads to 14.5% extra energy when it is charged to 4.4 V. It delivers 81% more discharge power and 65% more charge power while operating at 60°C. Furthermore, SEB-3 achieved >4000 cycles at 60°C while still showing signs of a healthy cell to continue operation. In addition, the high operational temperature facilitates thermal management. All these key advantages demonstrated here (high safety, high power on demand, long life, and easy thermal management) make SEB cells highly promising for widespread application to, e.g., the next-generation electric vehicles.

In the context of electric vehicles, introduction of the SEB yields a substantial gain in energy density and cost reduction at the pack level due to (i) simplified or entirely eliminated thermal management system; (ii) enhanced safety of SEB cells, thus enabling removal of some or all safety devices installed in a battery pack; and (iii) simplified battery management system due to SEB cells always operating at a single, constant temperature, rendering estimation of SOC, state of power, state of health, etc. oversimplified. We believe that 25 to 30% gain in energy density and 30% reduction in cost for SEB battery packs are possible without introducing new chemistry or cell manufacturing.

More broadly, the proposed strategy of passivating a battery cell for safety in idle conditions and then self-heating for high power before operation has a profound impact on future directions of battery materials development. Within the SEB framework, the high reactivity of active materials and electrolytes as well as of EEIs is no longer

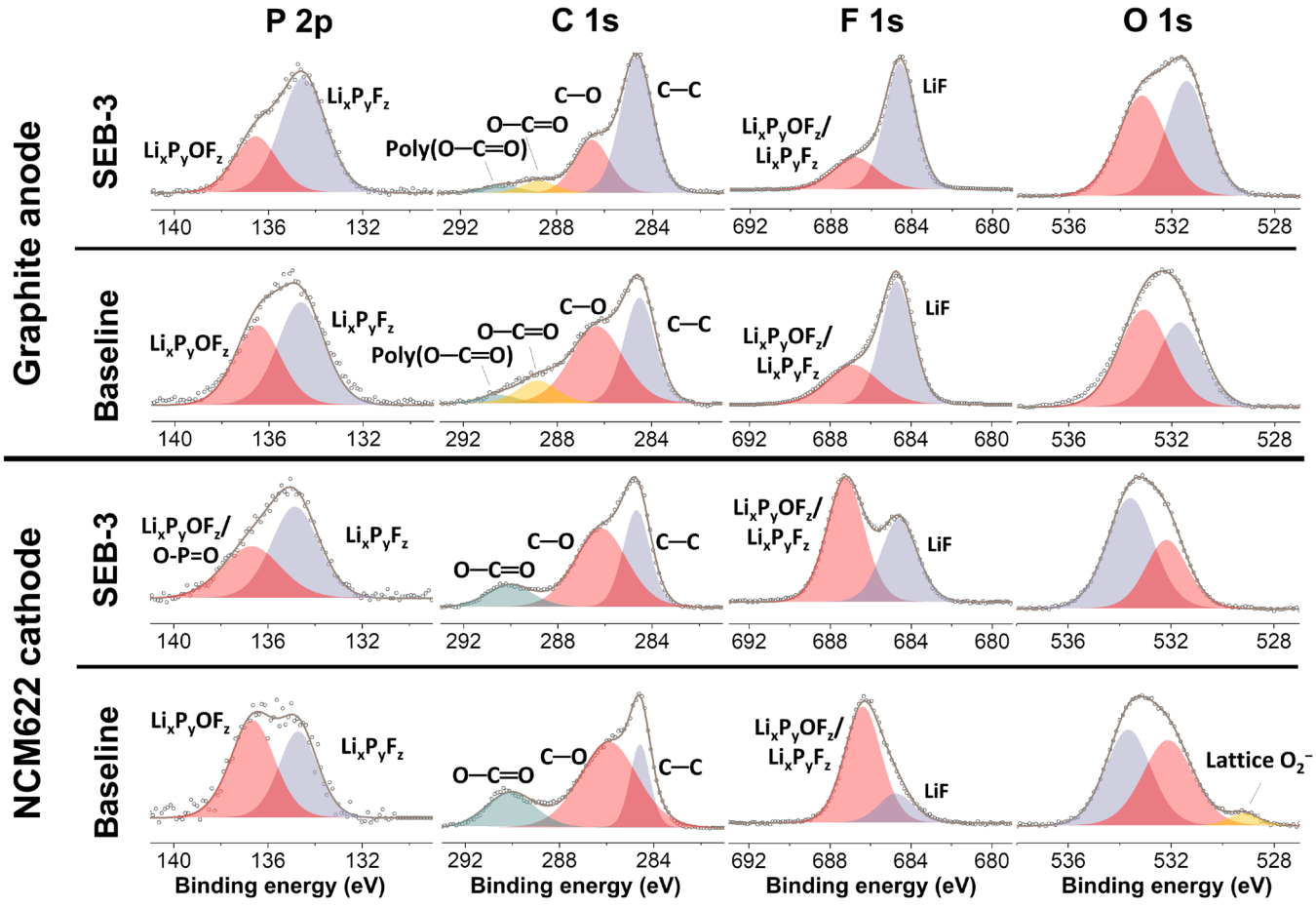

Fig. 6. XPS core spectra comparison for aged baseline and SEB-3 electrodes. The graphite and NCM622 electrodes are taken from the baseline cell after 956 cycles and the SEB-3 cell after 4021 cycles.

a requirement. The only requirement is stability at elevated temperatures. Such a design strategy will lead to dormant cell performance at low temperatures or even low power at room temperature, but all these deficiencies can be circumvented by the self-heating structure (*1*), which will take a SEB cell from low or room temperature to an elevated temperature suitable for high power output in tens of seconds. On the other hand, these SEB cells enjoy ultrahigh safety and ultralow degradation under all scenarios as well as robust cycling stability at elevated temperatures. We hope that this unconventional strategy will unleash a vast class of new materials for development of a disruptive generation of LIBs.

MATERIALS AND METHODS

We fabricated 2.8-Ah pouch cells using $LiNi_{0.6}Co_{0.2}Mn_{0.2}O_2$ (Umicore) for cathodes and graphite (Nippon Carbon) for anodes. The capacity ratio of negative to positive electrode, or NP ratio, was designed at 1.2. The 2.8-Ah pouch cell contains a stack of 20 anode and 19 cathode layers. A Celgard-2325 separator of 25 μm in thickness was used. The loadings of NMC622 on the positive electrode and graphite on the negative electrode were 10.5 and 6.6 mg/cm^2, respectively.

The cathodes were prepared by coating an N-methyl-2-pyrrolidone-based–based slurry onto 15-μm-thick Al foil, whose dry material consists of NCM622 (91.5 wt %), Super-P (TIMCAL) (4.1 wt %), and polyvinylidene fluoride (Arkema) (4.4 wt %) as a binder. The anodes were prepared by coating deionized water–based slurry onto 10-μm-thick Cu foil, whose dry material consists of graphite (95.4 wt %), Super-P (1.0 wt %), styrene-butadiene rubber (Zeon) (2.2 wt %), and carboxymethyl cellulose (Dai-Ichi Kogyo Seiyaku) (1.4 wt %).

One molar of $LiPF_6$ dissolved in EC/EMC (3:7 by wt) + 2 wt % VC was used as control electrolyte (BASF). One molar of $LiPF_6$ dissolved in a mixture of EC/EMC + 2 wt % VC was mixed in-house. To build SEB cells, 0.5 to 1.5 wt % TAP were mixed into the conventional electrolyte as additives.

Each pouch cell has a 110 mm × 56 mm footprint area, weighs 63 g, and has 2.8-Ah nominal capacity with a specific energy of 166 Wh/kg and an energy density of 310 Wh per liter. Discharge performance of the baseline and SEB cells at room temperatures is shown in fig. S7 as a function of C-rate.

Cycle aging tests of the pouch cells were performed using a Land instrument battery testing system (Model CT2001B, Land Instruments). A forced-air oven was used to control different ambient temperatures. For each aging cycle, the cell was charged to 4.2 V at a constant current of 2.8 A (1C-rate) and then charged at a constant voltage of 4.2 V until the current decreased to 0.14 A (C/20). After resting for 5 min, the cell was discharged to 2.8 V at a constant current of 2.8 A (1C-rate) followed by a final rest period of 5 min. When the aging cycle number reached a specific value (e.g., 403,

1006 cycles), the cell was cycled at a charge and discharge rate of C/3 to determine the capacity (designated as C/3 capacity) of the cell. For impedance tests at different temperatures, the cells were fully charged and then discharged at a rate of C/3 to 90% SOC. Impedance testing was performed with an AC voltage amplitude of 5 mV in the frequency range of 50 kHz to 0.005 Hz. For DCR test, the cells were fully charged and then discharged to 50% SOC at C/3-rate. A discharge rate of 5C and a charge rate of 3.75C were used to determine the value of $DCR_{Discharge}$ and DCR_{Charge}.

Calendar aging tests were performed at different ambient temperatures and SOCs. The forced-air oven was used to control different ambient temperatures. The cell voltage was kept constant, and the current was collected. When the calendar aging time reached a specific value (e.g., 25, 60, 120, and 180 days), the cell was cycled at a charge and discharge rate of C/3 to determine capacity of the cell. Then, impedance and DCR tests were conducted under the same conditions as that for the cycle-aged cells.

For the nail penetration test, the cell was fully charged (1C CCCV charge with a cutoff voltage of 4.2 V and a cutoff current of C/20). Thermocouples were placed at 10 mm to the geometry center of the cell and at the negative tab of the cell. The nail diameter is 5 mm, made of heat-resisting steel (point angle of the nail is 60°; nail surface is clean, without rust or oil). Rate of penetration was at 30 mm/s; the nail penetrated through the geometrical center of the electrode plane perpendicularly and stayed inside the cell. The observation time was 1 hour until the cell cooled down and the cell voltage dropped to nearly zero.

The SEM and XPS analyses were performed by first extracting the electrode samples from the fully discharged graphite/NCM622 pouch cells after cycling and washing 3× with EMC. XPS tests were conducted on a PHI VersaProbe II Scanning XPS Microprobe. The samples were loaded in a glove box and transferred into the instrument through a vacuum transfer vessel. SEM imaging was performed on an FEI Nova NanoSEM 630 SEM instrument.

SUPPLEMENTARY MATERIALS

Supplementary material for this article is available at http://advances.sciencemag.org/cgi/content/full/6/9/eaay7633/DC1

Fig. S1. Cycling behavior of LIB and SEB under over-charge conditions.
Fig. S2. Calendar life testing for LIB and SEB.
Fig. S3. Comparison of cell discharge performance.
Fig. S4. Optical comparison of fresh and aged electrodes.
Fig. S5. Elemental concentration of EEI layers.
Fig. S6. Discharge curves of the fresh baseline cell versus the aged cell.
Fig. S7. Comparison of C-rate discharge curves for the baseline LIB cell and the three SEB cells at room temperature.

REFERENCES AND NOTES

1. C.-Y. Wang, G. Zhang, S. Ge, T. Xu, Y. Ji, X.-G. Yang, Y. Leng, Lithium-ion battery structure that self-heats at low temperatures. *Nature* **529**, 515–518 (2016).
2. J. Xia, L. Madec, L. Ma, L. D. Ellis, W. Qiu, K. J. Nelson, Z. Lu, J. R. Dahn, Study of triallyl phosphate as an electrolyte additive for high voltage lithium-ion cells. *J. Power Sources* **295**, 203–211 (2015).
3. R. Jung, M. Metzger, F. Maglia, C. Stinner, H. A. Gasteiger, Oxygen release and its effect on the cycling stability of $LiNi_xMn_yCo_zO_2$ (NMC) cathode materials for Li-ion batteries. *J. Electrochem. Soc.* **164**, A1361–A1377 (2017).
4. S. Gaan, G. Sun, Effect of phosphorus flame retardants on thermo-oxidative decomposition of cotton. *Polym. Degrad. Stab.* **92**, 968–974 (2007).
5. L. de Biasi, A. O. Kondrakov, H. Geßwein, T. Brezesinski, P. Hartmann, J. Janek, Between scylla and charybdis: Balancing among structural stability and energy density of layered NCM cathode materials for advanced lithium-ion batteries. *J. Phys. Chem. C* **121**, 26163–26171 (2017).
6. H.-H. Ryu, K.-J. Park, C. S. Yoon, Y.-K. Sun, Capacity fading of Ni-rich $Li[Ni_xCo_yMn_{1-x-y}]O_2$ ($0.6 \leq x \leq 0.95$) cathodes for high-energy-density lithium-ion batteries: Bulk or surface degradation? *Chem. Mater.* **30**, 1155–1163 (2018).
7. C.-H. Shen, Q. Wang, H.-J. Chen, C.-G. Shi, H.-Y. Zhang, L. Huang, J.-T. Li, S.-G. Sun, In *situ* multitechnical investigation into capacity fading of high-voltage $LiNi_{0.5}Co_{0.2}Mn_{0.3}O_2$. *ACS Appl. Mater. Interfaces* **8**, 35323–35335 (2016).
8. R. Jung, F. Linsenmann, R. Thomas, J. Wandt, S. Solchenbach, F. Maglia, C. Stinner, M. Tromp, H. A. Gasteiger, Nickel, manganese, and cobalt dissolution from Ni-rich NMC and their effects on NMC622-graphite cells. *J. Electrochem. Soc.* **166**, A378–A389 (2019).
9. Y. Gao, Z. Yan, J. L. Gray, X. He, D. Wang, T. Chen, Q. Huang, Y. C. Li, H. Wang, S. H. Kim, T. E. Mallouk, D. Wang, Polymer–inorganic solid–electrolyte interphase for stable lithium metal batteries under lean electrolyte conditions. *Nat. Mater.* **18**, 384–389 (2019).
10. Y. Gao, Y. Zhao, Y. C. Li, Q. Huang, T. E. Mallouk, D. Wang, Interfacial chemistry regulation via a skin-grafting strategy enables high-performance lithium-metal batteries. *J. Am. Chem. Soc.* **139**, 15288–15291 (2017).
11. Y. Leng, S. Ge, D. Marple, X.-G. Yang, C. Bauer, P. Lamp, C.-Y. Wang, Electrochemical cycle-life characterization of high energy lithium-ion cells with thick $Li(Ni_{0.6}Mn_{0.2}Co_{0.2})O_2$ and graphite electrodes. *J. Electrochem. Soc.* **164**, A1037–A1049 (2017).
12. Q. Shi, G. Sheng, Electrolyte for lithium ion battery. CN103594729A (2014).
13. L. Ma, S. L. Glazier, R. Petibon, J. Xia, J. M. Peters, Q. Liu, J. Allen, R. N. C. Doig, J. R. Dahn, A guide to ethylene carbonate-free electrolyte making for Li-ion cells. *J. Electrochem. Soc.* **164**, A5008–A5018 (2017).
14. Y. Yamada, J. Wang, S. Ko, E. Watanabe, A. Yamada, Advances and issues in developing salt-concentrated battery electrolytes. *Nat. Energy* **4**, 269–280 (2019).

Acknowledgments

Funding: This work was partially supported by U.S. Department of Energy's Office of Energy Efficiency and Renewable Energy under award number DE-EE0008447. **Author contributions:** S.G. and C.-Y.W. developed the concept and wrote the manuscript. S.G. and R.S.L. designed and built the cells. S.G. built the test stand and carried out the performance characterization. T.L. carried out the nail penetration test. Y.L. performed the impedance analysis. Y.G. and Daiwei Wang carried out the XPS and SEM analysis. All authors contributed to development of the manuscript and to discussions as the project developed. **Competing interests:** The authors declare that they have no competing interests. **Data and materials availability:** All data needed to evaluate the conclusions in the paper are present in the paper and/or the Supplementary Materials. Additional data related to this paper may be requested from the authors.

Submitted 16 July 2019
Accepted 6 December 2019
Published 28 February 2020
10.1126/sciadv.aay7633

Citation: S. Ge, Y. Leng, T. Liu, R. S. Longchamps, X.-G. Yang, Y. Gao, D. Wang, D. Wang, C.-Y. Wang, A new approach to both high safety and high performance of lithium-ion batteries. *Sci. Adv.* **6**, eaay7633 (2020).